Available online at www.sciencedirect.com

ScienceDirect

Atmospheric Environment 42 (2008) 466–479

ATMOSPHERIC ENVIRONMENT

www.elsevier.com/locate/atmosenv

A Lagrangian particle model to predict the airborne spread of foot-and-mouth disease virus

D. Mayer[a], J. Reiczigel[a,b], F. Rubel[a,*]

[a]*Department of Natural Sciences, University of Veterinary Medicine Vienna, Veterinärplatz 1, A-1210 Vienna, Austria*
[b]*Department of Biomathematics and Informatics, Faculty of Veterinary Science, Szent István University, István u. 2, H-1078 Budapest, Hungary*

Received 17 August 2007; received in revised form 17 September 2007; accepted 24 September 2007

Abstract

Airborne spread of bioaerosols in the boundary layer over a complex terrain is simulated using a Lagrangian particle model, and applied to modelling the airborne spread of foot-and-mouth disease (FMD) virus. Two case studies are made with study domains located in a hilly region in the northwest of the Styrian capital Graz, the second largest town in Austria. Mountainous terrain as well as inhomogeneous and time varying meteorological conditions prevent from application of so far used Gaussian dispersion models, while the proposed model can handle these realistically. In the model, trajectories of several thousands of particles are computed and the distribution of virus concentration near the ground is calculated. This allows to assess risk of infection areas with respect to animal species of interest, such as cattle, swine or sheep. Meteorological input data like wind field and other variables necessary to compute turbulence were taken from the new pre-operational version of the non-hydrostatic numerical weather prediction model LMK (*Lokal-Modell-Kürzestfrist*) running at the German weather service DWD (*Deutscher Wetterdienst*). The LMK model provides meteorological parameters with a spatial resolution of about 2.8 km. To account for the spatial resolution of 400 m used by the Lagrangian particle model, the initial wind field is interpolated upon the finer grid by a mass consistent interpolation method. Case studies depict a significant influence of local wind systems on the spread of virus. Higher virus concentrations at the upwind side of the hills and marginal concentrations in the lee are well observable, as well as canalization effects by valleys. The study demonstrates that the Lagrangian particle model is an appropriate tool for risk assessment of airborne spread of virus by taking into account the realistic orographic and meteorological conditions.

Keywords: Lagrangian particle model; Atmospheric dispersion model; Foot-and-mouth disease; Airborne spread of virus; Veterinary epidemiology; Risk assessment

1. Introduction

Foot-and-mouth disease (FMD) is a highly contagious viral animal disease of significant economic impact (James and Rushton, 2002). The direct costs for the recent major FMD outbreaks in Great Britain 2001 have been estimated to about

*Corresponding author. Tel.: +43 1 25077 4325; fax: +43 1 25077 4390.
E-mail address: franz.rubel@vu-wien.ac.at (F. Rubel).

1352-2310/$ - see front matter
doi:10.1016/j.atmosenv.2007.09.069

Euro 4.7 billion, the indirect costs to about Euro 4.0–4.7 billion (Thompson et al., 2002). The constant threat of FMD was confirmed by the new outbreak in Great Britain reported on 3 August 2007, during the preparation phase of this paper. A multitude of epidemiological tools has been developed and applied to investigate the dynamics of the FMD outbreak in 2001. These tools comprise so-called epidemic models to predict the direct (contact based) transmission of FMD (Kao, 2002; Keeling, 2005) as well as dispersion models to predict the airborne spread of FMD (Gloster et al., 2003). In preparation for a potential FMD outbreak in Austria we describe the implementation of a high-resolution atmospheric dispersion model, i.e. a Lagrangian particle model to predict the airborne spread of FMD virus, and a first application to simulate multiple hypothetical FMD outbreaks in Austria. The Lagrangian dispersion model is designed to be an integrated part of a veterinary decision-support system so far comprising a data base of geo-referenced premises, a geographical information system (GIS) and a Gaussian dispersion model (Rubel and Fuchs, 2005).

1.1. Aims of study

Gloster and Alexandersen (2004) proposed several future research activities necessary to improve the estimation of airborne transmission of FMD virus. Here we focus on meteorological and modelling implications. These comprise the use of detailed parameters provided by state-of-the-art numerical weather prediction (NWP) models, the implementation of a sophisticated atmospheric dispersion model designed for continuously calculations of FMD virus concentrations of several simultaneous sources (infected premises) as well as the inclusion of detailed topography.

1.2. Dispersion models

With respect to dispersion modelling, two different approaches coexist. On the one hand, there are the widespread and in epidemiology established but with a lot of restriction afflicted Gaussian plume or puff models. They have been applied to study short-range (Cannon and Garner, 1999; Sørensen et al., 2000, 2001; Gloster et al., 2003, 2004a,b; Rubel and Fuchs, 2005) and long-range (Gloster et al., 1982, 2005; Sørensen, 1998) FMD virus transmission as well as the possible spread of FMD virus by the burning of animal carcases on open pyres (Champion et al., 2002; Jones et al., 2004). On the other hand, Lagrangian particle models can be applied to the full spectrum of inhomogeneous and time varying meteorological conditions even on non-flat terrains (Wilson and Sawford, 1996); however, they have been rarely applied to simulate FMD virus transmission. A recent application was presented by Gloster et al. (2003). In this study we describe the implementation of a Lagrangian dispersion model making use of the full information of NWP models concerning wind fields and turbulent fluxes.

According to Lamb et al. (1975) the spatio-temporal distribution of a substance's concentration $\overline{c}(\boldsymbol{x}, t)$ can be expressed by the emission rate $S(\boldsymbol{x}, t)$ and the conditional probability density $p(\boldsymbol{x}, t|\boldsymbol{x}', t')$ that a marked particle released at $(\boldsymbol{x}', t')$ will be found at $(\boldsymbol{x}, t)$:

$$\overline{c}(\boldsymbol{x}, t) = \int \int_0^t p(\boldsymbol{x}, t|\boldsymbol{x}', t') S(\boldsymbol{x}', t')\, \mathrm{d}t'\, \mathrm{d}\boldsymbol{x}', \tag{1}$$

where $\boldsymbol{x}$ and $\boldsymbol{x}'$ denote spatial coordinate vectors while t and t' denote time.

If the conditional probability density is supposed to be Gaussian and turbulence is homogeneous and stationary, Eq. (1) leads to Gaussian plume model (Seinfeld, 1975). In case of inhomogeneous turbulence conditions, however, no explicit function exists for p and, as a consequence, neither for $\overline{c}$. This more realistic case can only be studied by computing the distribution of concentration iteratively by means of numerical simulation.

The Lagrangian approach to handle particle dispersion appeared as early as in Taylor (1921), but that time turbulence was still assumed to be homogeneous. Due to the rapid development of computer technology Lagrangian particle models have been booming since the pioneer works of Smith (1968). Only a few years later, this random walk model was at first applied by Thomson (1971) and one of the first approaches considering complex topography was presented by Etling et al. (1986). Nowadays Lagrangian particle models can handle inhomogeneous turbulence and are applicable to all scales ranging from the evolution of galaxies to the movement of electrons in conductors (Zannetti, 1998). Recent applications comprise, for example, dispersion of atmospheric pollution (Da Costa Carvalho et al., 2007; Carvalhoa et al., 2005), airborne radionuclides from a nuclear power plant (Srinivas and Venkatesan, 2005) and bioaerosols (Pasken and Pietrowicz, 2005). There are two approaches for the calculation of the turbulent wind components. The first one uses the gradient of particle concentration (Lange, 1978), whereas the second one is based on a Monte Carlo method, in which the turbulent velocity is generated by a Markov process (Hanna, 1979). A detailed review of Lagrangian particle models describing various assumptions about turbulence and atmospheric stability can be found in Wilson and Sawford (1996).

In the present work, calculation of turbulence is based on a Monte Carlo method and in most respects like calculation of the turbulent wind speed and discretization of the domain it is similar to the Lagrangian particle model *LASAT* (Janicke, 2000). Significant differences exist in parameterizing quantities necessary to describe turbulence.

1.3. Wind flow models

Input wind data for a Lagrangian particle model are usually provided by an appropriate wind flow model in order to simulate dispersion due to the mean wind field. Wind flow models can be divided into two groups, namely prognostic and diagnostic models. The first group includes models that compute the time evolution of meteorological variables by integrating the equations of conservation at least for momentum, heat, mass and water. On the other side, models based on steady state solutions of the linearized Navier–Stokes equations (Jackson and Hunt, 1975) or on the analysis of measured or predicted wind data under physical constraints like mass conservation (Sherman, 1978) are assigned to diagnostic flow models. An overview of several flow models together with some implementations is given by Finardi et al. (1997).

In this work, a combination of a non-hydrostatic prognostic flow model and a mass consistent diagnostic flow model is used. Data from the first one are taken from *LMK* (*Lokal-Modell-Kürzestfrist*) operated at DWD (Baldauf et al., 2007). These wind fields have a horizontal resolution of $\Delta x \approx 2.8\,\text{km}$ where the influence of larger valleys and groups of mountains is already taken into account. The second one is a mass consistent wind model that interpolates or downscales the wind field from the NWP model to a resolution of $\Delta x \approx 400\,\text{m}$ by taking into account high-resolution topography. In this way even the effects of small valleys, single hills and passes on the wind flow are considered. The fine topography is taken from the high-resolution topographic database of the *Shuttle Radar Topography Mission* (SRTM) provided by NASA. This entire-world elevation data set has a horizontal resolution of 3 arcseconds that corresponds to $\Delta x \approx 60\,\text{m}$ for Central Europe.

The theoretical background of the mass consistent flow model was developed by Sasaki (1958). Originally, measured wind data are interpolated upon a regular grid and modified by the calculus of variations until divergence of the wind field reaches a minimum. An early and well-known application is the wind flow model *MATHEW* (Sherman, 1978). The mass consistent flow model implemented here is based on the paper of Magnusson (2005) and uses the terrain following coordinates of the NWP model of DWD to simplify the treatment of lower boundary conditions.

2. Model, parameterization and input data

2.1. Lagrangian particle model

To determine the distribution of concentration $\bar{c}(\boldsymbol{x}, t)$, some thousands of particle trajectories are computed. All trajectories are modelled independently of each other. The movement of a particle is determined by a velocity $\boldsymbol{v}$ that can be divided into a deterministic part $\bar{\boldsymbol{v}}$ called mean wind speed and a stochastic part $\boldsymbol{v}'$ called turbulent wind speed or wind fluctuation.

Both the position in space $\boldsymbol{x}$ and the turbulent wind speed $\boldsymbol{v}'$ are driven by a discrete-time Markov process. The position $\boldsymbol{x}$ at time t_{n+1} can be written as

$$\boldsymbol{x}_{n+1} = \boldsymbol{x}_n + \tau(\bar{\boldsymbol{v}}(\boldsymbol{x}_n) + \boldsymbol{v}'_{n+1}), \tag{2}$$

where $\tau = t_{n+1} - t_n$ denotes the time step.

The mean wind speed $\bar{\boldsymbol{v}}$ is taken from the downscaled NWP data. The turbulent wind speed $\boldsymbol{v}'_{n+1}$ is further divided into two parts, namely an autoregressive component $\boldsymbol{\Psi} \cdot \boldsymbol{v}'_n$ and a partially random component $\boldsymbol{\omega}$:

$$\boldsymbol{v}'_{n+1} = \boldsymbol{\Psi}(\boldsymbol{x}_n) \cdot \boldsymbol{v}'_n + \boldsymbol{\omega}. \tag{3}$$

As a consequence of anisotropic turbulence and the so-caused interactions between the spatial components, the factor $\boldsymbol{\Psi}$ in the Markov process is a tensor of second order and plays the role of an autocorrelation coefficient.

Now, we have to specify $\boldsymbol{\omega}$. Also this velocity component can be split into two components. The first is the drift velocity $\boldsymbol{W}$ that prevents the accumulation of particles in regions with lower turbulence and the second is a Gaussian random number $\boldsymbol{r}$ with mean 0 and variance 1 that is weighted with the tensor $\boldsymbol{\Lambda}$ for the purpose of energy conservation.

$$\boldsymbol{\omega} = \boldsymbol{W}(\boldsymbol{x}_n) + \boldsymbol{\Lambda}(\boldsymbol{x}_n) \cdot \boldsymbol{r}. \tag{4}$$

All quantities mentioned above can be deduced from the components of the mean wind field $\overline{u}$, $\overline{v}$ and $\overline{w}$, the components of the wind fluctuation σ_u, σ_v and σ_w, the friction velocity u_* and the Lagrangian time scales T_u, T_v and T_w. The tensor $\boldsymbol{\Lambda}$ can be expressed as the Cholesky decomposition of the tensor $\boldsymbol{\Omega}$ defined as

$$\boldsymbol{\Omega} = \boldsymbol{\Sigma} - \boldsymbol{\Psi} \cdot \boldsymbol{\Sigma} \cdot \boldsymbol{\Psi}^{\mathrm{T}}, \tag{5}$$

where $\boldsymbol{\Psi}^{\mathrm{T}}$ denotes the transpose of $\boldsymbol{\Psi}$, and $\boldsymbol{\Sigma}$ contains the covariances of the wind fluctuations in order to consider horizontal and vertical interactions:

$$\boldsymbol{\Sigma} = \begin{pmatrix} \sigma_u^2 & 0 & -u_*^2 \\ 0 & \sigma_v^2 & 0 \\ -u_*^2 & 0 & \sigma_w^2 \end{pmatrix}. \tag{6}$$

The factor $\boldsymbol{\Psi}$ of the Markov process can be written as a function of a tensor $\boldsymbol{\Phi}$ whose diagonal elements correspond to the reciprocal Lagrangian time scales and the other elements can be expressed by the wind fluctuations and the friction velocity in the following way:

$$\boldsymbol{\Psi} = (\boldsymbol{I} - \tfrac{1}{2}\tau\boldsymbol{\Phi}) \cdot (\boldsymbol{I} + \tfrac{1}{2}\tau\boldsymbol{\Phi})^{-1}, \tag{7}$$

where $\boldsymbol{I}$ is the identity matrix and

$$\boldsymbol{\Phi} = \begin{pmatrix} \dfrac{1}{T_u} & 0 & -\dfrac{u_*^2}{T_w\sigma_w^2} \\ 0 & \dfrac{1}{T_v} & 0 \\ -\dfrac{u_*^2}{T_u\sigma_u^2} & 0 & \dfrac{1}{T_w} \end{pmatrix}. \tag{8}$$

To complete this section we have to define the drift velocity $\boldsymbol{W}$. This vector consists of the factor of the Markov process $\boldsymbol{\Psi}$ and the divergence of the variance tensor $\boldsymbol{\Sigma}$:

$$\boldsymbol{W} = \tfrac{1}{2}\tau(\boldsymbol{I} + \boldsymbol{\Psi}) \cdot (\boldsymbol{\nabla} \cdot \boldsymbol{\Sigma}), \tag{9}$$

where $\boldsymbol{\nabla}$ is the Nabla-operator. Using the Gauss' Theorem, the divergence of the tensor can be calculated by integrating the flux through the surface of the grid cell.

2.2. Parameterization of turbulent quantities

In the literature, there exist several approaches for the parameterization of the above-mentioned turbulent quantities σ_u, σ_v, σ_w, u_*, T_u, T_v and T_w (Kerschgens et al., 2000). While most of these approaches assume a discrete classification of the atmospheric stability, there are some supporting a continuous quantification of stability in terms of the Monin–Obukhov length L.

Friction velocity u_* can be computed directly from its defining equation:

$$u_* = [\overline{(w'u')}_0^2 + \overline{(w'v')}_0^2]^{1/4}, \tag{10}$$

where u', v' and w' are the components of the turbulent wind speed $\boldsymbol{v}'$. The quantities $\overline{(w'u')}_0$ and $\overline{(w'v')}_0$ represent the surface values of the fluxes of kinematic impulse that, except for a factor, come from the NWP model.

The Monin–Obukhov length L is used to classify the stability and is defined as follows:

$$L = -\frac{u_*^3\Theta}{\kappa g\overline{(w'\Theta')}_0}, \tag{11}$$

where $\kappa = 0.4$ is the von Kármán constant, Θ is the potential temperature near the surface and $\overline{(w'\Theta')}_0$ is the kinematic heat flux at ground level (also provided by the weather prediction model, except for a factor). The boundary layer is supposed to be stable if $L>0$, unstable if $L<0$ and neutral if $|L| \to \infty$.

Mixing layer height h plays two important roles. First, h defines the vertical extension for particle dispersion; furthermore it is a scaling parameter for the wind fluctuations and Lagrangian time scales. In this work, h is calculated using the concept of the (critical) Bulk–Richardson number Ri^{c} according to Holtslag et al. (1995) and Vogelzang and Holtslag (1996):

$$h - z_1 = Ri^{\mathrm{c}} \frac{(\overline{u}(h) - \overline{u}(z_1))^2 + (\overline{v}(h) - \overline{v}(z_1))^2 + 100u_*^2}{g/\Theta_v(z_1)[\Theta_v(h) - \Theta_{vs}]}, \tag{12}$$

where $\overline{u}(h)$ and $\overline{v}(h)$ are components of the mean wind speed $\overline{\boldsymbol{v}}$ at height h while $20 \leqslant z_1 \leqslant 50\,\mathrm{m}$. Furthermore Θ_v is the virtual potential temperature, $Ri^{\mathrm{c}} = 0.25$ the critical Bulk–Richardson number. The additional term Θ_{vs} in Eq. (12) takes into account the effect of convective air parcels by consideration of the excess temperature Θ_T near the surface (Troen and Mahrt, 1986):

$$\Theta_{vs} = \Theta_v(s) + \Theta_T = \Theta_v(s) + \frac{(8.5\overline{w'\Theta'_v})_0}{(u_*^3 + 0.6w_*^3)^{1/3}}, \quad (13)$$

where $\Theta_v(s)$ is the virtual potential temperature at the surface and $(\overline{w'\Theta'_v})_0$ is the buoyancy flux at the surface. According to Potty et al. (2000) this flux can be derived from the heat flux $(\overline{w'\Theta'})_0$ and the moisture flux $(\overline{w'q'})_0$:

$$(\overline{w'\Theta'_v})_0 = (\overline{w'\Theta'})_0 + 0.6078[\Theta(\overline{w'q'})_0 + q(\overline{w'\Theta'})_0], \quad (14)$$

where q is the specific humidity. This quantity as well as the moisture and heat fluxes can be taken from the weather prediction model. In Eq. (13) w_* is the convective scaling velocity:

$$w_* = \left(\frac{g}{\Theta}(\overline{w'\Theta'})_0 h\right)^{1/3}, \quad (15)$$

with g being the acceleration due to gravity.

Vertical profiles of the wind fluctuations $\sigma_u(z)$, $\sigma_v(z)$ and $\sigma_w(z)$ can be calculated from the mixing layer height h, friction velocity u_* and convective scaling velocity w_*, also depending on atmospheric stability. For unstable to neutral atmospheric stability the recommendation of Kerschgens et al. (2000) is followed with the modification that the exponential height dependence in Eqs. (16) and (17) is here applied to the whole expression.

$$\sigma_u = [(2.4u_*)^3 + (0.59w_*)^3]^{1/3} \exp\left\{-\frac{z}{h}\right\}, \quad (16)$$

$$\sigma_v = [(1.8u_*)^3 + (0.59w_*)^3]^{1/3} \exp\left\{-\frac{z}{h}\right\}, \quad (17)$$

$$\sigma_w = \left[\left(1.3u_* \exp\left\{-\frac{z}{h}\right\}\right)^3 + \left(1.3\left(\frac{z}{h}\right)^{1/3}\left(1-0.8\frac{z}{h}\right)w_*\right)^3\right]^{1/3}. \quad (18)$$

For stable layering the recommendation of Kerschgens et al. (2000) is applied without modification:

$$\sigma_u = 2.4u_* \exp\left\{-\frac{z}{h}\right\}, \quad (19)$$

$$\sigma_v = 1.8u_* \exp\left\{-\frac{z}{h}\right\}, \quad (20)$$

$$\sigma_w = 1.3u_* \exp\left\{-\frac{z}{h}\right\}. \quad (21)$$

From the wide variety of expressions for the Lagrangian time scales T_u, T_v and T_w we have chosen the one by Luhar and Britter (1989), which is valid for the whole spectrum of atmospheric layering:

$$T_u = \frac{2\sigma_u^2}{C_0\varepsilon}, \quad T_v = \frac{2\sigma_v^2}{C_0\varepsilon}, \quad T_w = \frac{2\sigma_w^2}{C_0\varepsilon}, \quad (22)$$

where $C_0 = 5.7$ is the Kolmogorov constant (Ley, 1982) and ε is the rate of dissipation of the turbulent kinetic energy. Concerning ε, for unstable to neutral stratifications the recommendation by Luhar and Britter (1989) is followed:

$$\varepsilon = \max\left\{\frac{u_*^3}{\kappa z}\left[\left(1-\frac{z}{h}\right)^2 + 2.5\kappa\frac{z}{h}\right] + \frac{w_*^3}{h}\left[1.5 - 1.3\left(\frac{z}{h}\right)^{1/3}\right], \frac{u_*^3}{\kappa z}\right\}, \quad (23)$$

whereas for stable atmospheric layering the approach according to Wyngaard (1975) is applied:

$$\varepsilon = \frac{u_*^3}{\kappa z}\left(1 + 4\frac{z}{L}\right). \quad (24)$$

All these parameterizations assure continuous changeovers even in cases with changing spatial and temporal stability conditions.

2.3. *Input data from NWP model*

The meteorological input data for the Lagrangian particle model are provided by the LMK model (Steppeler et al., 2003; Baldauf et al., 2007) of the German Weather Service (DWD). Since June 2006 this non-hydrostatic model runs in a pre-operational testing phase and is planned to complete the previous operating *Global Modell* (GME) and the therein nested *Lokal-Modell Europa* (LME) in the course of the year 2007. This model covers the area of Germany, the alpine countries Austria and Switzerland and parts of the surrounding countries.

A considerable innovation is the increased resolution from $\Delta x = 7$ km (LME) up to $\Delta x = 2.8$ km (LMK); the increase in the number of vertical layers from 40 to 50 as well as the reduction of the time step of the numerical integration from $\Delta t = 40$ s to $\Delta t = 30$ s. Because of a forecast duration of 18 h and its initialization frequency of 8 times a day, the LMK model belongs to the group of very short-range NWP models. A further innovation is the explicit consideration of deep moist convection whereby phenomena like super- and multi-cell thunderstorms or squall-lines can be taken into account. Furthermore, interactions with fine-scale topography like severe downslope winds, Foehn-Storms or fog can be predicted.

The Lagrangian particle model presented here uses the three-dimensional fields of horizontal and vertical wind components, temperature, pressure, specific moisture as well as the two-dimensional surface fields of momentum, sensible and latent heat fluxes with a temporal resolution of $\Delta t = 1\,\mathrm{h}$.

2.4. Mass consistent wind field data

The mass consistent interpolation of the initial mean wind field $\overline{\boldsymbol{v}}_0$ (from the LMK model) to a fine grid taking into account the topography must satisfy two constraints. The resulting mean wind field $\overline{\boldsymbol{v}}$ should be as similar as possible to the initial wind field $\overline{\boldsymbol{v}}_0$ but with a minimal divergence integrated over the whole domain:

$$\int \left[\alpha_x^2(\overline{u}-\overline{u}_0)^2 + \alpha_y^2(\overline{v}-\overline{v}_0)^2 + \alpha_z^2(\overline{w}-\overline{w}_0)^2 + 2\lambda\left(\frac{\partial \overline{u}}{\partial x} + \frac{\partial \overline{v}}{\partial y} + \frac{\partial \overline{w}}{\partial z}\right)\right] \mathrm{d}V = \mathrm{Min}. \tag{25}$$

Here λ plays the role of a Lagrangian multiplier, $\alpha_x = \alpha_y$ and α_z are the horizontal and vertical transmission coefficients, also called Gaussian precision moduli. These specify the relative importance of adjustment of horizontal and vertical wind components and can be expressed as functions of the horizontal and vertical turbulent wind fluctuations σ_u and σ_w (Magnusson, 2005). So, the stability dependent tendency to overflow or to circulate around an orographic formation can be simulated in a realistic way. Using the calculus of variations Eq. (25) can be transformed into a partial differential equation of second order for the Lagrangian multiplier λ.

$$\frac{1}{\alpha_x^2}\frac{\partial^2 \lambda}{\partial x^2} + \frac{1}{\alpha_y^2}\frac{\partial^2 \lambda}{\partial y^2} + \frac{1}{\alpha_z^2}\frac{\partial^2 \lambda}{\partial z^2} = -\left(\frac{\partial \overline{u}_0}{\partial x} + \frac{\partial \overline{v}_0}{\partial y} + \frac{\partial \overline{w}_0}{\partial z}\right). \tag{26}$$

The right-hand side of Eq. (26) is the divergence of the initial wind field $\overline{\boldsymbol{v}}_0$. Solving the discretized form of Eq. (26) numerically for λ, the following wind components are obtained:

$$\overline{u} = \overline{u}_0 + \frac{1}{\alpha_x^2}\frac{\partial \lambda}{\partial x}, \quad \overline{v} = \overline{v}_0 + \frac{1}{\alpha_y^2}\frac{\partial \lambda}{\partial y}, \quad \overline{w} = \overline{w}_0 + \frac{1}{\alpha_z^2}\frac{\partial \lambda}{\partial z}. \tag{27}$$

Lower boundary conditions can be taken into account more easily if the problem is formulated in terrain following coordinates x, y and η satisfying

$$\eta(x,y,z) = s\left[\frac{z - z_{\mathrm{G}}(x,y)}{s - z_{\mathrm{G}}(x,y)}\right], \tag{28}$$

where s is the altitude, at which the influence of terrain vanishes and z_{G} is the elevation of the orography. The numerical value of $s = 11\,357\,\mathrm{m}$ is specified by the NWP model and has been adopted to the mass consistent wind model for compatibility reasons.

The mass consistent interpolated wind field possesses all observable features of local wind systems like canalization through valleys, an increase in velocity over ridges and stability dependent tendencies to overflow or circulate around hills.

The procedure was implemented for three-dimensional domains of $60 \times 60 \times 30$ grid points corresponding to an area of $25 \times 25\,\mathrm{km}^2$ (Fig. 1).

2.5. Virus emission rates and infectious dose

Virus emission of infected animals is expressed in terms of *Tissue Culture Infectious Dose* (TCID_{50}), that is the dose of virus needed to infect a tissue culture with a probability of 50%. In most cases, this dose is quoted in terms of the common logarithm and is referenced to a time period of 1 day. On this account, a commonly used abbreviation is $\log_{10}\mathrm{TCID}_{50}\,\mathrm{d}^{-1}$.

Every species varies in virus emission as well as in the critical value of the concentration that leads to an infection. Because of their greater respiratory volume cattle are the most endangered animals, whereas swine are least vulnerable, requiring higher concentrations to be infected. Table 1 depicts a selection of emission rates as well as the critical concentrations for infection of cattle, swine and sheep for FMD virus serotype O_1 after Sørensen et al. (2000). Note that emission rates depend on the virus serotype, the species and the day of clinical signs, respectively. For simplification, case studies demonstrating the performance of the new Lagrangian particle model have been calculated with constant emission rates. Simulating real-world applications, the determination of realistic emission rates is a challenging task.

The Lagrangian particle model works with variable discrete time steps of the order of $\Delta t = 5\,\mathrm{s}$. Thus, every time step a number of n simulated particles are released. The virus dose that one particle represents is then $q = Q/n$, where Q is the virus emission rate in $\mathrm{TCID}_{50}\,\mathrm{s}^{-1}$. By discretizing the spatial domain into grid cells with volume V,

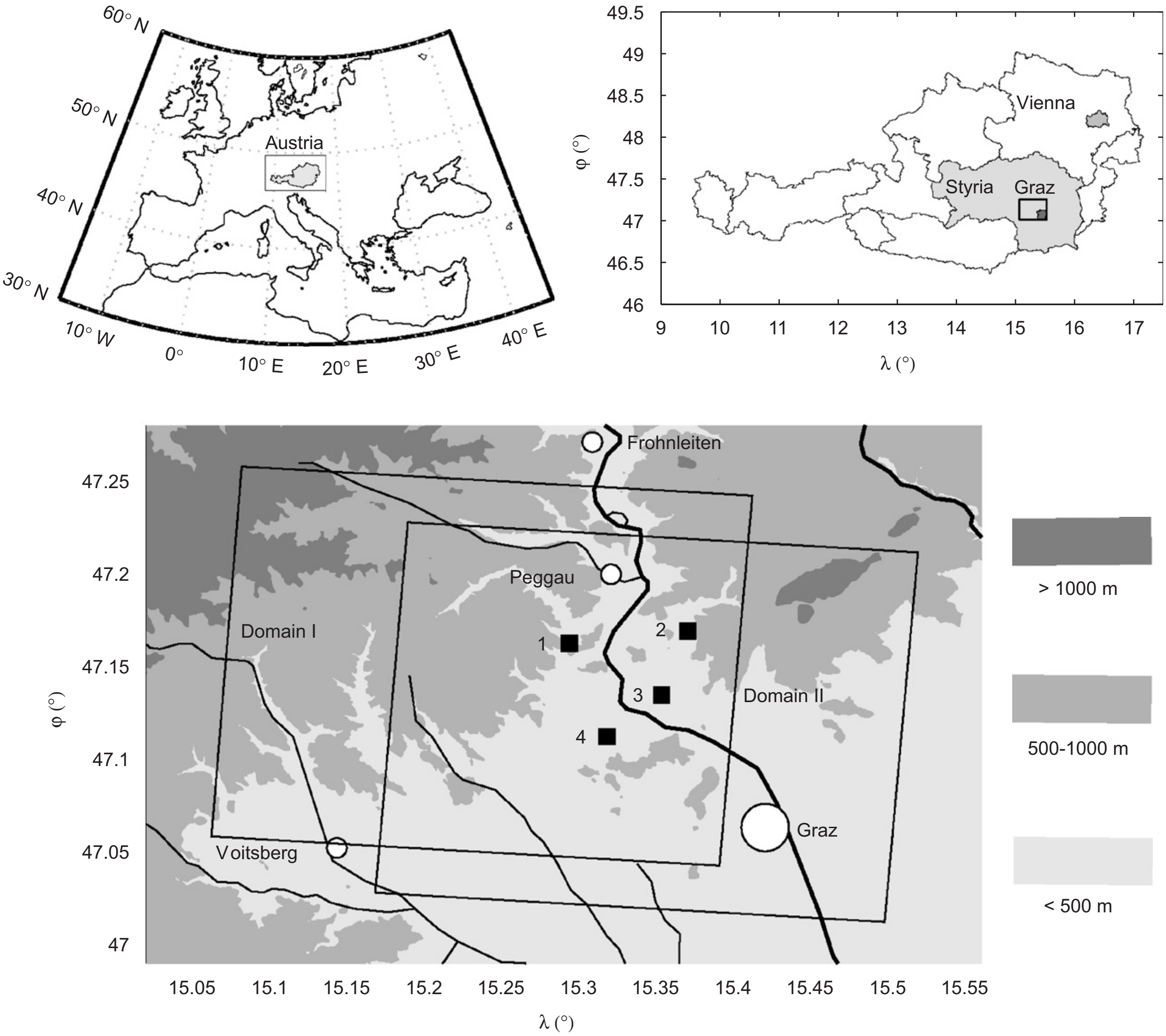

Fig. 1. Map with Lagrangian model domains (black frames), towns (white disks), hypothetically infected farms (black squares) and rivers (black lines).

Table 1
Virus emission rates (Garner and Cannon, 1995) and critical values of concentrations for different species after Sørensen et al. (2000)

Species	Cattle	Swine	Sheep
Emission rate ($\log_{10}$ $TCID_{50}$ d^{-1})	5.06	7.16	4.94
Critical concentration ($TCID_{50}$ m^{-3})	0.06	7.70	1.11

indexed by i, j and k, distribution of concentration c can be computed as follows:

$$c_{i,j,k} = \frac{q\sum_p t_p}{V_{i,j,k}T}, \tag{29}$$

where t_p is the time particle p stays in the cell i, j, k and T is the accumulation period usually 1 h or 1 day.

3. Case studies

3.1. Domains

As domains for the case studies, two partially overlapping regions with an extension of $25 \times 25\,km^2$ were selected northwest of Graz, the Styrian capital and second largest town of Austria. These diversified regions comprise a large valley, moderately ranged mountains and a basin. From north to south the *Mur*-Valley crosses the domains.

This valley enlarges twice, firstly to the *Gratwein-Gratkorner* basin and in the south to the *Grazer* field. The altitude of the hills and mountains ranges from 300 to 1200 m, at the border of one domain, some tops reach a level of 1700 m.

The entire region depicted in Fig. 1 comprises a total of 2959 farms with 17 563 swine, 8842 goats and sheep and 39 203 cattle. This is equivalent to a density of 2.2 farms km^{-2} or 13.1 swine km^{-2}, 6.6 sheep and goat km^{-2} and 29.2 cattle km^{-2}.

In both case studies the same farms were assumed to be affected (with the same number of infected cattle, swine and sheep). Differences come from the different meteorological conditions on the two selected days, such as mean wind field, turbulence and variation in time of the atmospheric layering. The geographical coordinates of the affected farms, the number of infected animals and the entire emission rates of FMD-virus in units of $TCID_{50}\,s^{-1}$ are shown in Table 2. The latter are calculated from the single emission rates given in Table 1 multiplied by the total number of animals located at the infected farms.

Four farms with different topographical environments have been chosen. Whereas farms 3 and 4 are situated in the basin, Farm 1 is located in a small side valley and Farm 2 in the hilly area.

3.2. *Case study I: 16 September 2006*

The surface chart from the German weather service (DWD, 2007) depicts the general weather situation of Europe for 16 September 2006, 12:00 UTC (Fig. 2). Whereas a stable anticyclone is located over Eastern Europe, an occlusion has already crossed the Alps and reaches the easterly lowland of Austria. The domain of the case study is influenced by the warm sector with winds from southeast in the morning. In the afternoon storm

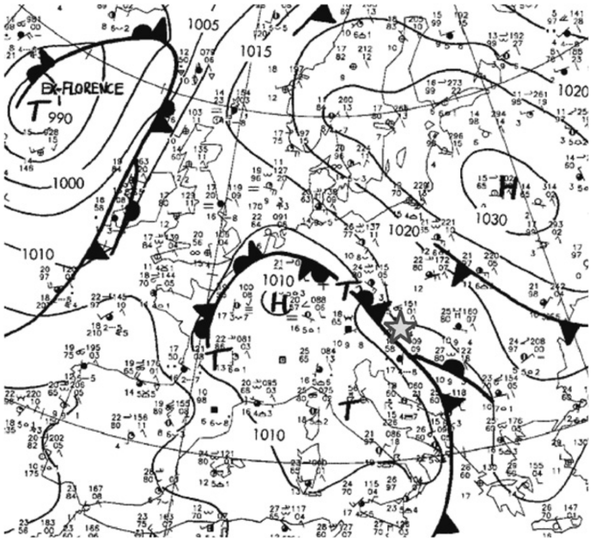

Fig. 2. Surface weather chart for Europe, 16 September 2006, 12:00 UTC (DWD, 2007). The location of the study domain is marked by a gray star.

rainfall is caused by the point of occlusion that is centered over the domain. For this reason airborne spread of virus is only simulated till 13:00 UTC.

In the morning the atmosphere is layered stably. In the lowlands and mountains (except for the valleys) the wind blows slightly and comes from easterly directions (Fig. 3a). In contrast, valleys are able to modify the wind flow considerably. After atmospheric stratification has changed from stable to neutral, wind shifts to east to southeast and its speed has generally increased to $|\boldsymbol{v}| > 5\,m\,s^{-1}$ whereby local wind systems in valleys have disappeared (Fig. 3b). Orographic elevations are now overflown, whereas, as a consequence of stable layering, wind flow circulated around the hills in the morning.

Fig. 4 depicts snapshots of virus spread visualized by more than 25 000 simulated particles at 9:00 UTC (a), 11:00 UTC (b), 12:00 UTC (c) and 13:00 UTC (d). According to the vertical layer of the NWP model, wherein the particles are located, they are colored differently in ascending order from yellow, to green, cyan, blue, magenta, red and black. It is self-evident that only particles of the lowest layer (yellow) can be inhaled by animals. Only particles located within the yet thin mixing layer are shown. The circulating flow around the hill can be observed in Fig. 4a, whereas canalizing effects are illustrated in Fig. 4d near Farm 2.

The atmospheric layering has a considerable effect on the shape of the risk area. Very stable

Table 2
Coordinates of affected farms, number of infected animals and total FMD virus emission rates

Farm	1	2	3	4
λ (°E)	15.2936	15.3702	15.3532	15.3178
φ (°N)	47.1625	47.1729	47.1345	47.1121
Cattle	29	8	2	45
Sheep	0	0	29	0
Swine	4	8	26	15
Emission rate ($TCID_{50}\,s^{-1}$)	708	1349	4382	2569

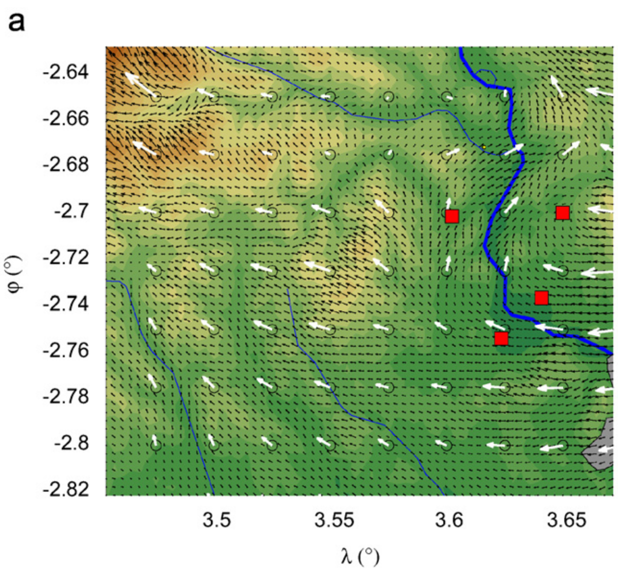

Fig. 3. Surface wind field for 16 September 2006, 09:00 UTC (a) and 12:00 UTC (b) depicting the initial wind field from NWP model (white arrows) and the mass consistent downscaled wind field used by the Lagrangian particle model (black arrows). Note that wind vectors are scaled proportional to the grid size. The positions of infected farms are marked by red squares.

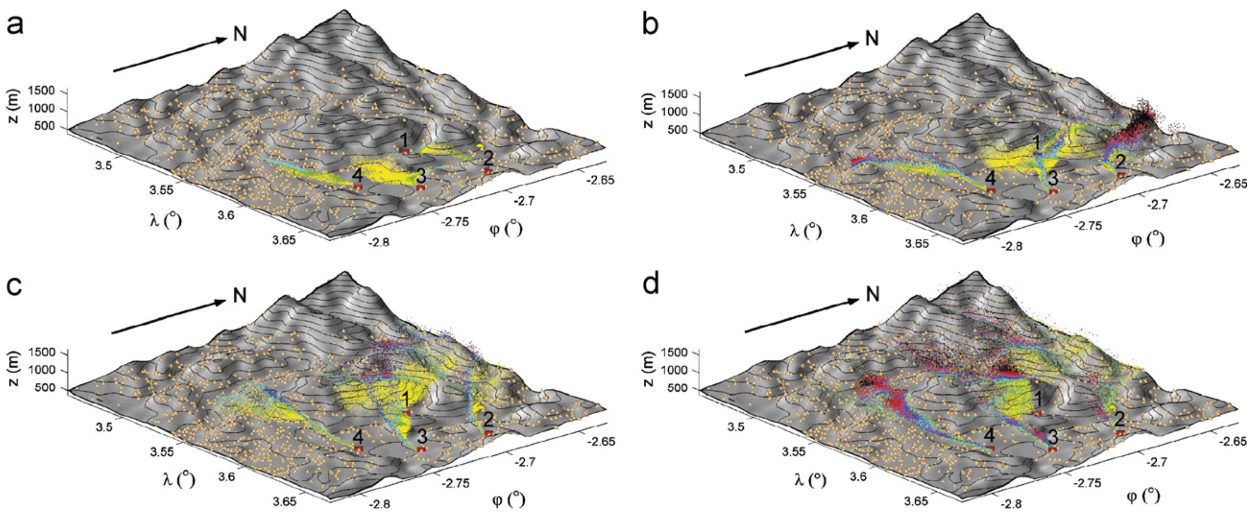

Fig. 4. Snap-shot of virus plumes for 16 September 2006, 9:00 UTC (a), 11:00 UTC (b), 12:00 UTC (c) and 13:00 UTC (d). Red squares indicate for the positions of infected farms, brown points for the more than 1000 susceptible farms in the $25 \times 25\,\mathrm{km}^2$ model domain. Yellow particles are located in the lowest 10 m above ground. Green, cyan, blue, magenta and black points mark viruses at higher vertical layers.

stratifications may produce narrow areas with high doses and therefore high risk for all three species, like, e.g. those in Fig. 5a near Farms 3 and 4 located in the basin. Another consequence of the stable layering is that the wind flow circulates around a hill instead of overflowing it, like, e.g. near Farm 3 in Fig. 5a.

Three hours later atmospheric layering turns to neutral and hills are overflown now. Another effect that cannot be handled by Gaussian dispersion models appears, the lee effect. As shown in Fig. 5b, upwind sides of hills are much more affected than lee sides. Even far away from virus sources (particularly Farm 2) exposed hill territories can be risk areas for cattle. On the other hand, areas that are situated closer to the source but do not face it are quite safe even for cattle. A further consequence of the neutral layering is the widening of the risk area

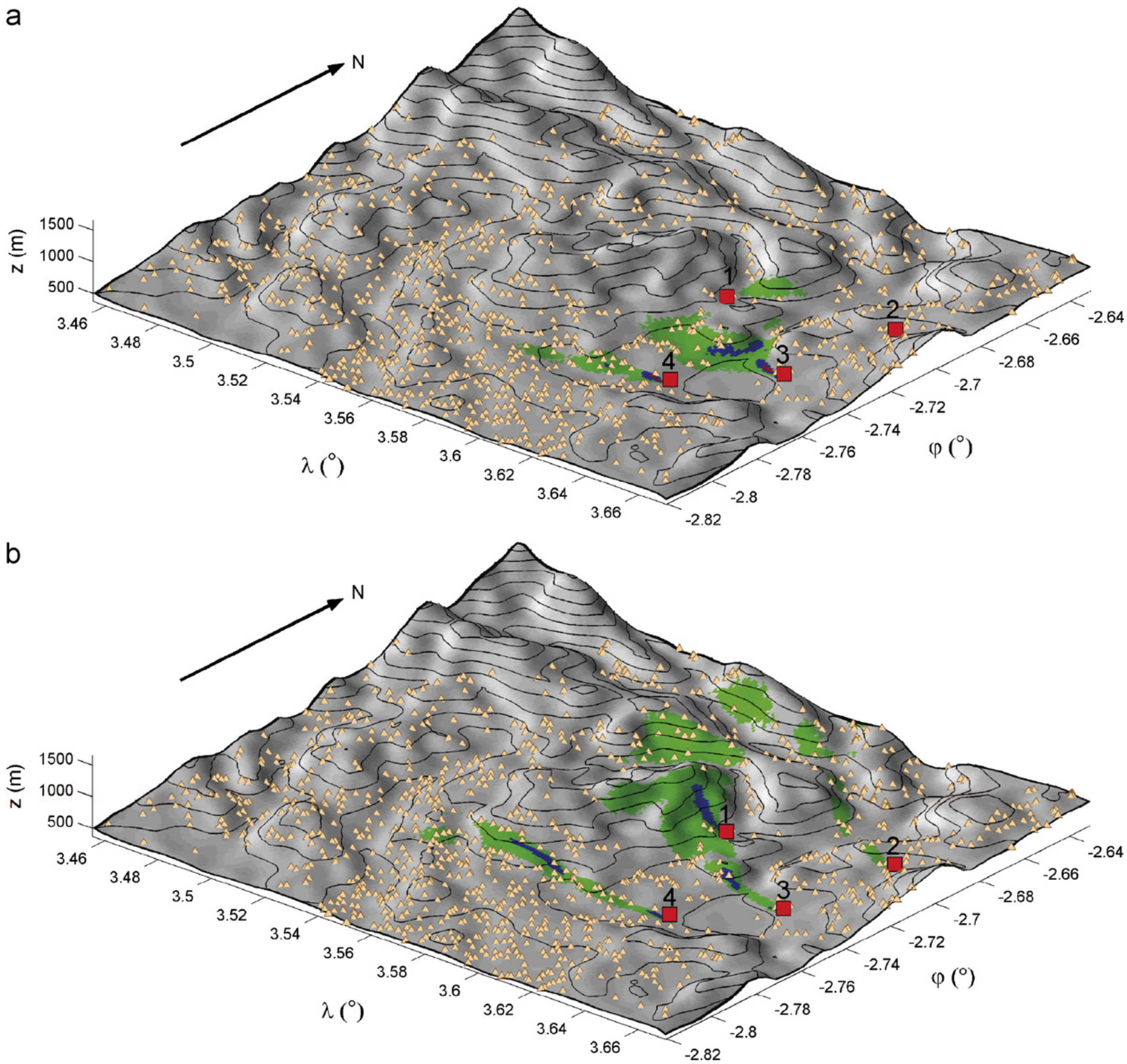

Fig. 5. Risk areas for cattle (green), sheep (blue) and swine (red) based on the critical concentrations given in Table 1. Date 16 September 2006, accumulation period 9:00–10:00 UTC (a) and 12:00–13:00 UTC (b). Numbered red squares mark the location of infected farms, brown points all other farms. Domain size $25 \times 25\,\mathrm{km}^2$.

but with decreasing exposure so that swine are only at risk if they reside directly in the neighborhood of the affected farms. Apart from the lee effects, canalizing effect of valleys can be observed, e.g. in case of the virus plume emitted by Farm 3 in Fig. 5b.

3.3. Case study II: 1 November 2006

A long cold front reaching from Spain to Russia included in the strong northern upper airflow has reached the Alps and displaces the up to now quite stable anticyclone toward the southeast (Fig. 6). At the back side polar air masses are transported to Central Europe leading to the first onset of winter even in the lowlands.

The early morning of 1 November 2006 was characterized by a gentle breeze with a ground wind speed of $|\boldsymbol{v}| < 1\,\mathrm{m\,s^{-1}}$. No prevailing direction of wind can be noticed, nearly every valley has its own local wind system. Due to the stable atmospheric stratification, mixing layer height is still low.

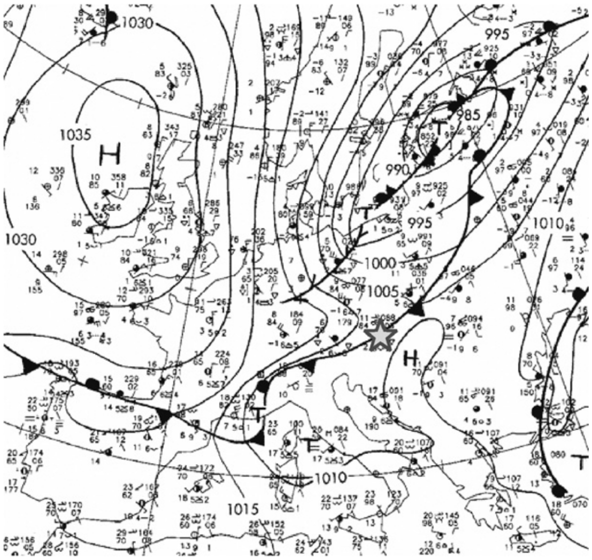

Fig. 6. Surface weather chart for Europe, 1 November 2006, 12:00 UTC (DWD, 2007). The location of the study domain is marked by a gray star.

A snap-shot of the morning wind conditions at 6:00 UTC is shown in Fig. 7a.

In front of the approaching significant cold front from the north 4 h later, the wind breezes up ($|\boldsymbol{v}| \approx 5\,\mathrm{m\,s^{-1}}$) and shifts to northern directions (Fig. 7b). The very stable atmospheric layering is removed by a neutral layering whereby an increase of the mixing layer height from $h \leqslant 100$ m in the early morning to $h \approx 1500$ m in front of the approaching cold front can be observed.

A snapshot of the position of nearly 40 000 simulated FMD virus particles at 5:00 UTC, 8:00 UTC, 10:00 UTC and 11:00 UTC is shown in Fig. 8. Yellow points correspond to viruses located in the lowest vertical layer, i.e. those able to infect animals. A pronounced lee effect can be observed in the virus plume of Farm 3 (Fig. 8c) and of Farm 4 (Fig. 8d). Distant hills are exposed to viruses while other hill sides that do not face the affected farm are quite safe areas even if they are located closer to it. Plumes emitted by farms 1 and 2 (Fig. 8c and d) remain aloof from the ground after having crossed the ambient hills, preventing inhalation of virus by farm animals.

Finally, Fig. 9 depicts areas within which different species are under risk to be infected due to airborne spread of FMD virus. The risk areas depicted in Fig. 9 may be calculated for any accumulation period. Here an accumulation period of 8 h was selected.

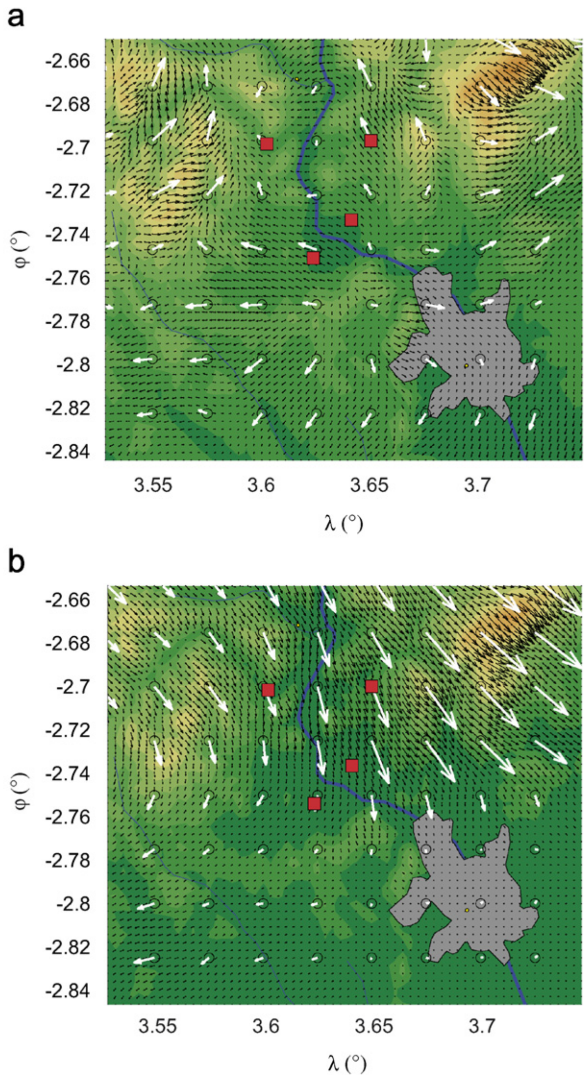

Fig. 7. Surface wind field for 1 November 2006, 06:00 UTC (a) and 10:00 UTC (b) depicting the initial wind field from NWP model (white arrows) and the mass consistent downscaled wind field used by the Lagrangian particle model (black arrows). Note that wind vectors are scaled proportional to the grid size. Red squares show the positions of infected farms, the gray area indicates urban agglomeration of Graz.

4. Discussion and future prospects

An upgrade from Gaussian plume and puff models to Lagrangian particle models allows an extension of the range of application of airborne spread of FMD virus. Whereas Gaussian plume models require temporally and spatially constant and isotropic wind and turbulence conditions and can deal only with a moderate topography with some oversimplifications,

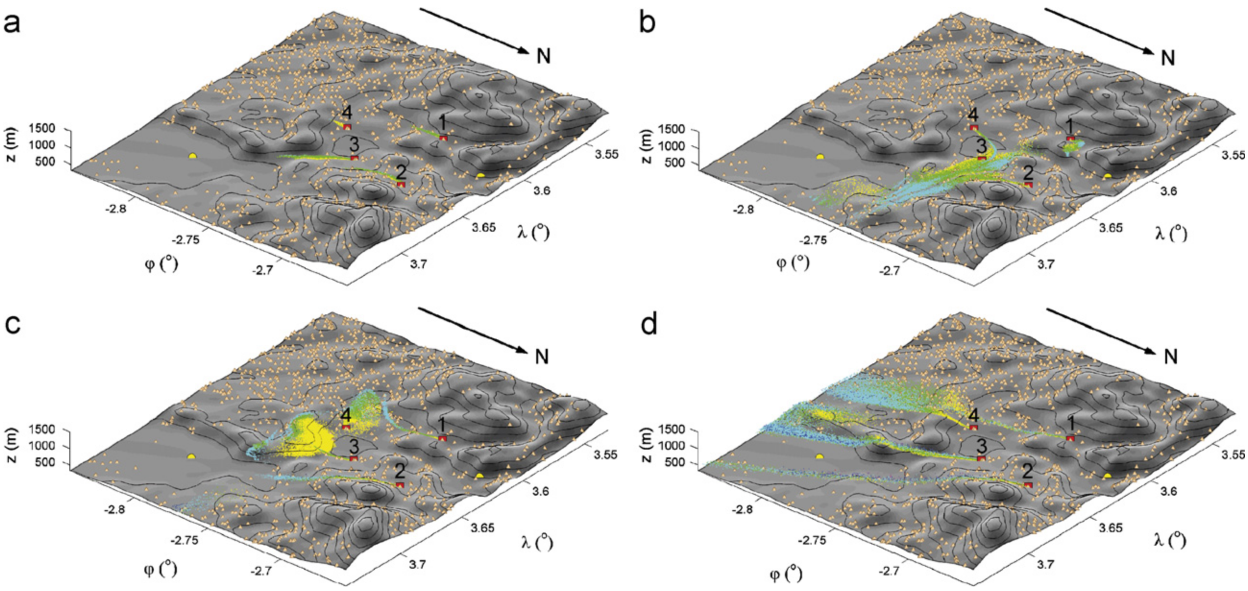

Fig. 8. Snap-shot of virus plumes for 1 November 2006, 5:00 UTC (a), 8:00 UTC (b), 10:00 UTC (c) and 11:00 UTC (d). Red squares indicate the positions of infected farms, brown points the more than 1000 susceptible farms in the $25 \times 25\,\mathrm{km}^2$ model domain. Yellow particles are located in the lowest 10 m above ground. Green and cyan points mark viruses at higher vertical layers.

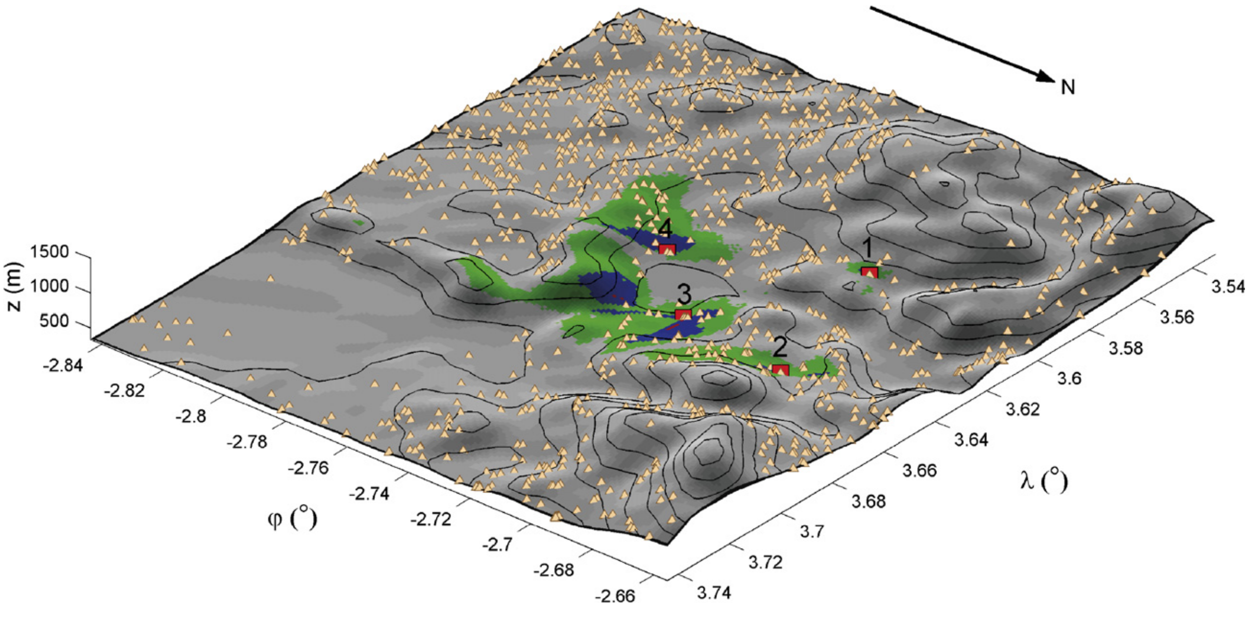

Fig. 9. Risk areas for cattle (green), sheep (blue) and swine (red), based on the critical concentrations given in Table 1. Date 1 November 2006, accumulation period 4:00–12:00 UTC. Numbered red squares mark the location of infected farms, brown points all other farms. Domain size $25 \times 25\,\mathrm{km}^2$.

Lagrangian particle models are applicable to nearly all real situation like such characteristic phenomena as vertical wind shear, wind fields modified by the topography, as well as spatiotemporally varying mixing layer heights.

As demonstrated in this work, the use of a mass consistent wind flow model combined with high-resolution elevation data allows for investigation of the consequences of topography such as lee and canalization effects on the shape of risk areas.

Having a more precise knowledge of those farms that are really affected, the control of FMD epidemics may be improved.

In the above two preliminary case studies, a temporally constant virus emission rate of four hypothetically infected farms was assumed. If considering real-world epidemics of longer time periods, it is necessary to use time dependent emission rates, which should be updated at least daily by using information from veterinarians in the field. In addition, the effect of environmental parameters like air temperature, humidity, precipitation and radiation on the biological activity of the virus must be considered. Simulating longer time periods requires also larger domains with much more grid points. Further, it may be necessary to simulate the emission of FMD virus from much more than four simultaneously infected farms.

Nevertheless, the proposed Lagrangian particle model for the estimation of airborne spread of FMD virus is a first step to improve estimations previously based on Gaussian dispersion models. A more detailed description comprising vertical profiles of meteorological input parameters such as temperature, humidity, wind speed, height of the boundary layer, dissipation rate of the turbulent kinetic energy, turbulent wind fluctuations, Lagrangian time scales as well as animations of the virus plumes depicted in Figs. 4 and 8 are available at http://i115srv.vu-wien.ac.at/staff/mayer/Lagrange/Lagrange.htm.

Acknowledgments

This research was supported by research Grant PP 1500 0007 of the University of Veterinary Medicine Vienna. The German weather service (DWD) provided the meteorological input data for the case studies. We thank Udo Voigt (DWD) for assistance with data transfer and Dr Michael Baldauf (DWD) for interpreting NWP model output.

References

Baldauf, M., Helmert, K., Hassler, B., Stephan, K., Klink, S., Schraff, C., Seifert, A., Foerstner, J., Reinhardt, T., Lenz, C.-J., 2007. The new very short range forecast model LMK for the convection-resolving scale. Geophysical Research Abstracts 9, A-09141.

Cannon, R.M., Garner, M.G., 1999. Assessing the risk of wind-borne spread of foot-and-mouth disease in Australia. Environment International 25, 713–723.

Carvalhoa, J.C., Túllio, M., de Vilhenab, M.B., 2005. Pollutant dispersion simulation for low wind speed condition by the ILS method. Atmospheric Environment 39, 6282–6288.

Champion, H.J., Gloster, J., Mason, I.S., Brown, R.J., Donaldson, A.I., Ryall, D.B., Garland, A.J.M., 2002. Investigation of the possible spread of foot-and-mouth disease virus by the burning of animal carcases on open pyres. Veterinary Record 151, 593–600.

Da Costa Carvalho, J., Degrazia, G.A., Anfossi, D., De Campos, C.R.J., Roberti, D.R., Kerr, A.S., 2007. Lagrangian stochastic dispersion modelling for the simulation of the release of contaminants from tall and low sources. Meteorologische Zeitschrift 11, 89–97.

DWD, 2007. Online Surface Weather Chart Archive. ⟨http://www2.wetter3.de/Archiv/archiv_dwd.html⟩.

Etling, D., Preuss, J., Wamser, M., 1986. Application of random walk model to turbulent diffusion in complex terrain. Atmospheric Environment 20, 741–747.

Finardi, S., Morselli, M.G., Jeannet, P., 1997. Wind flow models over complex terrain for dispersion calculations. COST Action 710, Preprocessing of meteorological data for dispersion modelling. Report of Working Group 4, 12–25.

Garner, M.G., Cannon, R.M., 1995. Potential for wind-borne spread of foot-and mouth disease virus in Australia. A Report Prepared for the Australian Meat Research Corporation. p. 88. ⟨http://www.daff.gov.au/__data/assets/pdf_file/0007/159541/fmdwind.pdf⟩.

Gloster, J.H., Alexandersen, S., 2004. New directions: airborne transmission of foot-and-mouth disease virus. Atmospheric Environment 38, 503–505.

Gloster, J., Sellers, R.F., Donaldson, A.I., 1982. Long distance transport of foot-and-mouth disease virus over sea. Veterinary Record 110, 47–52.

Gloster, J., Champion, H.J., Sørensen, J.H., Mikkelsen, T., Ryall, D.B., Astrup, P., Alexandersen, S., Donaldson, A.I., 2003. Airborne transmission of foot-and-mouth disease virus from Burnside Farm, Heddonon-the-Wall, Northumberland during the 2001 epidemic in the United Kingdom. Veterinary Record 152, 525–533.

Gloster, J.H., Ryall, D., Brown, A., 2004a. The 2001 UK epidemic of foot-and-mouth disease—a meteorological review: Part 1. Weather 59, 8–11.

Gloster, J.H., Ryall, D., Brown, A., 2004b. The 2001 UK epidemic of foot-and-mouth disease—a meteorological review: Part 2. Weather 59, 43–45.

Gloster, J., Freshwater, A., Sellers, R.F., Alexandersen, S., 2005. Re-assessing the likelihood of airborne spread of foot-and-mouth disease at the start of the 1967–1968 UK foot-and-mouth disease epidemic. Epidemiology and Infection 133, 767–783.

Hanna, S.R., 1979. Some statistics of Lagrangian and Eulerian wind fluctuations. Journal of Applied Meteorology 18, 518–525.

Holtslag, A.A.M., van Meijgaard, E., De Roy, W.C., 1995. A Comparison of boundary layer diffusion schemes in unstable conditions over land. Boundary-Layer Meteorology 76, 69–95.

Jackson, P.S., Hunt, J.C.R., 1975. Turbulent wind flow over a low hill. Quarterly Journal of the Royal Meteorological Society 101, 929–955.

James, A.D., Rushton, J., 2002. The economics of foot and mouth disease. Revue Scientifique et Technique Office International des Epizooties 21, 637–644.

Janicke, L., 2000. A random walk model for turbulent diffusion. Reports on Environmental Physics 1, 1–10 ⟨http://www.janicke.de/data/bzu/bzu-001-01.pdf⟩.

Jones, R., Kelly, L., French, N., England, T., Livesey, C., Wooldridge, M., 2004. Quantitative estimates of the risk of new outbreaks of foot-and-mouth disease as a result of burning pyres. Veterinary Record 154, 161–165.

Kao, R.R., 2002. The role of mathematical modelling in the control of the 2001 FMD epidemic in the UK. Trends in Microbiology 10, 279–286.

Keeling, M.J., 2005. Models of foot-and-mouth disease. Proceedings of the Royal Society B 272, 1195–1202.

Kerschgens, M.J., Nölle, C., Martens, R., 2000. Comments on turbulence parameters for the calculation of dispersion in the atmospheric boundary layer. Meteorologische Zeitschrift 9, 155–164.

Lamb, R.G., Chen, W.H., Seinfeld, J.H., 1975. Numerico-empirical analyses of atmospheric diffusion theories. Journal of the Atmospheric Sciences 32, 1794–1806.

Lange, R., 1978. ADIPC—a three-dimensional particle-in-cell model for the dispersal of atmospheric pollutants and its comparison to regional tracer studies. Journal of Applied Meteorology 17, 320–329.

Ley, A.J., 1982. A random walk simulation of two dimensional turbulent diffusion in the neutral surface layer. Atmospheric Environment 16, 2799–2808.

Luhar, A.K., Britter, R.E., 1989. A random walk model for dispersion in inhomogeneous turbulence in a convective boundary layer. Atmospheric Environment 23, 1911–1989.

Magnusson, L., 2005. Development and validation of a new mass-consistent model using terrain influenced coordinates. Institutionen för Geovetenskaper. ⟨www.geo.uu.se/luva/exarb/2005/Linus_Magnusson.pdf⟩.

Pasken, R., Pietrowicz, J., 2005. Using dispersion and mesoscale meteorological models to forecast pollen concentrations. Atmospheric Environment 39, 7689–7701.

Potty, K.V.J., Mohanty, U.C., Raman, S., 2000. Simulation of boundary layer structure over the Indian summer monsoon trough during the passage of a depression. Journal of Applied Meteorology 40, 1241–1254.

Rubel, F., Fuchs, K., 2005. A decision-support system for real-time risk assessment of airborne spread of the foot-and-mouth disease virus. Methods of Information in Medicine 44, 590–595.

Sasaki, Y., 1958. An objective analysis based on the variational method. Journal of the Meteorological Society of Japan 36, 77–88.

Seinfeld, J.H., 1975. Air pollution—physical and Chemical Fundamentals. McGraw-Hill, New York.

Sherman, C., 1978. A mass-consistent model for wind fields over complex terrain. Journal of Applied Meteorology 117, 312–319.

Smith, F.B., 1968. Conditioned particle motion in a homogeneous turbulent field. Atmospheric Environment 2, 491–508.

Sørensen, J.H., 1998. Sensitivity of the DERMA long-range Gaussian dispersion model to meteorological input and diffusion parameters. Atmospheric Environment 32, 4195–4206.

Sørensen, J., Mackay, D., Jensen, C., Donaldson, A., 2000. An integrated model to predict the atmospheric spread of FMD virus. Epidemiology and Infection 124, 577–590.

Sørensen, J.H., Jensen, C.O., Mikkelsen, T., Mackay, D.K.J., Donaldson, A.I., 2001. Modelling the atmospheric dispersion of foot-and-mouth disease virus for emergency preparedness. Physics and Chemistry of the Earth Part B 26, 93–97.

Srinivas, C.V., Venkatesan, R., 2005. A simulation study of dispersion of air borne radionuclides from a nuclear power plant under a hypothetical accidental scenario at a tropical coastal site. Atmospheric Environment 39, 1497–1511.

Steppeler, J., Doms, G., Schättler, U., Bitzer, H.W., Gassmann, A., Damrath, U., Gregoric, G., 2003. Meso-gamma scale forecasts using the nonhydrostatic model LM. Meteorology and Atmospheric Physics 82, 7596.

Taylor, G.I., 1921. Diffusion by continuous movements. Proceedings of the London Mathematical Society 20, 196–202.

Thomson, R., 1971. Numeric calculation of turbulent diffusion. Quarterly Journal of the Royal Meteorological Society 97, 93–98.

Thompson, D., Muriel, P., Russell, D., Osborne, P., Bromley, A., Rowland, M., Creigh-Tyte, S., Brown, C., 2002. Economic costs of the foot and mouth disease outbreak in the United Kingdom in 2001. Revue Scientifique et Technique Office International des Epizooties 21, 675–687.

Troen, I., Mahrt, L., 1986. A simple model of the atmospheric boundary layer. Boundary-Layer Meteorology 37, 129–149.

Vogelzang, D.H.P., Holtslag, A.A.M., 1996. Evolution and model impacts of alternative boundary layer formulations. Boundary-Layer Meteorology 81, 245–269.

Wilson, J.D., Sawford, B.L., 1996. Review of Lagrangian stochastic models for trajectories in the turbulent atmosphere. Boundary-Layer Meteorology 78, 191–210.

Wyngaard, J.C., 1975. Modeling the planetary boundary layer-extension to the stable case. Boundary-Layer Meteorology 9, 441–460.

Zannetti, P., 1998. Air pollution modeling: theories, computational methods and available software. Computational Mechanics Publications, Southampton, UK.